

PLASMA CONDENSATION IN SOLAR CORONAL LOOPS

I. BASIC PROCESSES

D.A.N. Müller^{1,2}, V.H. Hansteen², and H. Peter¹

¹Kiepenheuer-Institut für Sonnenphysik, Schöneckstr. 6, D-79104 Freiburg, Germany, Email: dmueller@kis.uni-freiburg.de, peter@kis.uni-freiburg.de

²Institute of Theoretical Astrophysics, University of Oslo, P.O. Box 1029, Blindern N-0315, Oslo, Norway, Email: Viggo.Hansteen@astro.uio.no

ABSTRACT

In the first part of this work, we report numerical calculations of the condensation of plasma in short coronal loops, which has several interesting physical consequences. We propose a connection between small, cool loops, which presumably constitute the solar transition region, and prominences in the sense that the same physical mechanism governs their dynamics, namely the onset of instability and runaway cooling due to strong radiative losses. We show that the temporal evolution of these loop models exhibits a cyclic pattern of chromospheric evaporation, condensation, motion of the condensation region to either side of the loop, and finally loop reheating with a period of 4000 – 8000 s for a loop of 10 Mm length. Furthermore, we have synthesized transition region lines from these calculations which show strong periodic intensity variations, making condensation in loops a candidate to account for observed transient brightenings of solar transition region lines. Remarkably, all these dynamic processes take place for a heating function which is *constant* in time and has a simple exponential height dependence. In the second part of this work (Müller et al., 2003b), we apply this concept to large coronal loops.

Key words: Sun: corona; Sun: transition region; Sun: UV radiation.

1. INTRODUCTION

Since Skylab, loops have been recognized as a vital ingredient in coronal structure and coronal energetics. Indeed, one could imagine that the corona is entirely composed of nested loops with varying lengths, temperatures, heating rates, and activity levels. A nested structure of low-lying cool loops was suggested by Dowdy et al. (1986) to explain the temperature dependence of the emission measure. Thus, building an understanding of loop energetics is obviously a desirable objective. The main components in the energy balance of *static* loops were identified by Rosner et al. (1978): They consist of the unknown heat-

ing, thermal conduction and radiative losses in the loop itself and at the transition region/chromosphere boundary. Roughly speaking one can understand static loop behavior quite well by assuming that the heat deposited by the heating mechanism in the corona is largely conducted back towards the chromosphere where it is radiated away. Due to the strong temperature dependence of the thermal conduction coefficient, this scenario almost inevitably leads to apex loop temperatures of roughly 1 MK bounded by a geometrically small transition region as the temperatures fall towards 10^4 K and chromospheric densities at the loop footpoints. Variations in the heating rate are dealt with in this type of loop by chromospheric evaporation or coronal condensation such that the radiative losses at the top of the chromosphere balance the thermal conductive flux from above (Hansteen, 1993). This behavior is almost independent of the details of the heat deposition - as long as radiative losses near the loop apex are not an important factor in the energy budget.

Clear as the model above seems, serious difficulties are encountered as soon as loop model predictions are confronted with the observations themselves. These difficulties are various and sundry (Mariska, 1992) but might be summarized as follows: The differential emission measures predicted by the models gives a much lower line emission from the lower transition region, below 10^5 K, than what is observed (alternatively one could say that the line emission from the upper transition region, above 10^5 K, is predicted much too high). In addition it is very difficult to account for the pervasive *average* red shift of up to 10 km/s seen in lower transition region lines and blue-shifts in the upper transition region and low corona (Peter & Judge, 1999).

Several proposals have been put forward to answer the difficulties outlined above. Dowdy et al. (1986) suggested a two-component transition region, consisting of magnetic funnels and a nested structure of low-lying, cool coronal loops. This new class of static loop solutions had been discussed by Antiochos & Noci (1986). Cally & Robb (1991) argued, however, that these cool loop solutions were unstable, and Cally (1990) proposed turbulent thermal conduction as an alternative hypothesis to explain the enhanced transition region emission. As for the

spectral diagnostics of transition region lines, loop dynamics due to downward-propagating magneto-acoustic waves were shown to be a candidate to account for the pervasive redshifts (Hansteen, 1993).

Numerous mechanisms of coronal heating have been proposed (e.g. wave heating, nanoflares, magnetic reconnection), but independent of the detailed process of energy release there is now observational evidence that coronal loops are predominantly heated at the footpoints (Aschwanden et al., 2000, 2001). With heating concentrated near the loop footpoints it is no longer certain that sufficient energy to counter radiative losses is deposited near the loop apex. In fact, for such loops static solutions with a hot midpoint may no longer exist as the radiative loss rate increases strongly in the loop center when the temperature decreases towards $T \approx 2 \cdot 10^5$ K. If the magnetic field topology is such that the loop has a dip in the center, footpoint heating can lead to the condensation of plasma in the loop center and hence give rise to prominence formation (Antiochos et al., 1999). It was also found by Antiochos et al. (2000) that this type of prominence formation shows a cycle of formation, motion, and destruction. Recently, it was demonstrated by Karpen et al. (2001) that the condition of a “dipped” geometry is indeed not a necessary condition for prominence formation in long loops (their work describes a loop of 340 Mm length). A key element in their prominence scenario is the large ratio of loop length to the damping length of the heating function, and the authors argue that shorter loops with a smaller ratio should therefore behave differently. We present numerical calculations which show that, depending on the damping length of the heating function, condensation is also possible in short, cool coronal loops. We study the evolution of these loops, discuss static as well as dynamic solutions and finally calculate the time-dependent emission of transition region lines arising from this model.

2. NUMERICAL MODEL

We numerically solve the time-dependent hydrodynamic equations for conservation of mass, momentum and energy in one spatial dimension, coupled with the ionization rate equations for several elements and self-consistent radiative losses (cf. Hansteen, 1993; Müller et al., 2003a, for details). The modeled plasma is subjected to gravitational acceleration equal to that found on the solar surface. Thermal conduction, radiative losses and a coronal heating term are included in the energy equation. The internal energy, e , is calculated as the sum of the thermal and internal energy including only ionization states, the contribution from the excitation energy is negligible. The thermal conduction is set to $F_c = \kappa_0 T^{5/2} dT/dz$ (Spitzer, 1962) with $\kappa_0 = 1.1 \times 10^{-11} \text{ W m}^{-1} \text{ s}^{-1} \text{ K}^{-7/2}$.

Some of the metals are treated by assuming ionization equilibrium and then deriving an *a priori* radiative loss curve as a function of electron temperature. On the other hand radiative losses from the ions specifically mentioned in this study, i.e. losses from hydrogen, helium, carbon and oxygen, are computed consistently with full time-dependent rate equations, accounting for non-equilibrium

ionization.

2.1. Loop heating

In order to parametrize the energy input into the coronal loop, we specify the energy flux amplitude at the footpoints of the loop, F_{m0} , and assume a mechanical heat flux that is constant up to a height z_1 and then decreases for $z \geq z_1$ as

$$F_m(z) = F_{m0} \exp[-(z - z_1)/H_m] \quad (1)$$

with a damping length H_m . We will vary H_m between 0.25 and 3.25 Mm in the models presented below. For the mechanical energy flux we use $F_{m0} = c \cdot 150 \text{ W/m}^2$ with the normalization constant $c = 1/(1 - \exp[-(z_{\text{cutoff}} - z_1)/H_m])$, $z_{\text{cutoff}} = z_1 + 5 \cdot H_m$ (similar to the one used by Hansteen & Leer (1995)) and set $z_1 = 1.75 \text{ Mm}$ for a loop of 10 Mm length. The heating rate, i.e. the energy deposition per unit time and unit volume, is given by the divergence of the energy flux, $Q_m = -\nabla F_m$. We consider a loop of low- β plasma and assume a constant cross section of the loop, i.e. $A = A_0 = \text{const}$. This parametrization of the heating function was first suggested by Serio et al. (1981) and seems to be supported by recent observations (Aschwanden et al., 2000, 2001) as well as by numerical models (Gudiksen & Nordlund, 2002). Special care was taken to normalize the heating rate to a given energy flux in order to separate effects from changes of the amplitude of the energy flux to changes in its spatial distribution.

3. RESULTS: CONDENSATION DUE TO THERMAL INSTABILITY

3.1. Initial state

Our model coronal loop has a total length of 10 Mm, consisting of a semicircular arch of 8 Mm length and a vertical stretch of 1 Mm length at both ends. At the base we set a total particle density of $n_{\text{base}} = 8.8 \cdot 10^{20} \text{ m}^{-3}$. This density corresponds (very) roughly to a height of $h = 605 \text{ km}$ above $\tau_{500\text{nm}} = 1$ in the Vernazza et al. (1981) quiet sun model. The ionization degree of hydrogen is $\approx 0.3\%$ at this height in our model. The base temperature is set to $T_{\text{base}} = 7000 \text{ K}$. In the chromosphere, the temperature remains constant while the density falls off exponentially with a scale height of about 190 km until the transition region is encountered at 1.6 Mm. Here the temperature rises rapidly reaching 10^5 K at 1.63 Mm and $5 \cdot 10^5 \text{ K}$ at 2.81 Mm. The loop apex temperature is $6.55 \cdot 10^5 \text{ K}$. Energy losses by radiation are $L_{\text{rad}} \approx 10^{-4} \text{ W m}^{-3}$ in the coronal and transition region portions of the loop while conductive losses to the top of the chromosphere account for $\nabla Q \approx 8 \cdot 10^{-4} \text{ W m}^{-3}$, i.e. the loop is essentially a “hot loop” in that the energetics are dominated by conduction (see Müller et al., 2003a, for more details on the initial state).

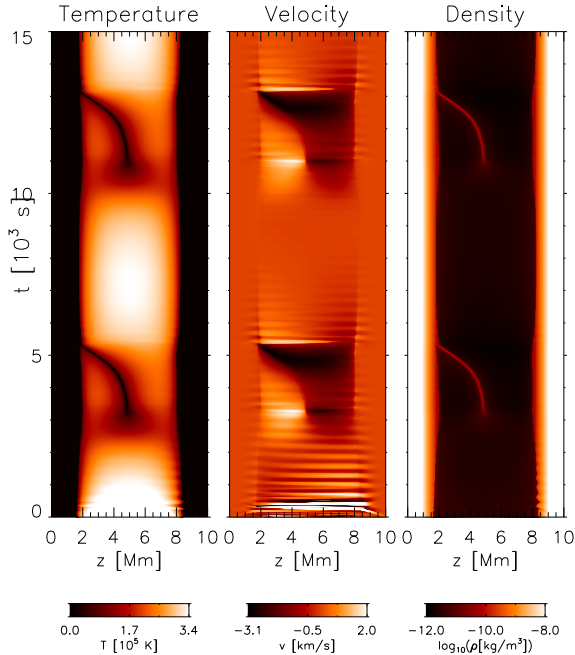


Figure 1. Temporal evolution of temperature (left), velocity (center), and density (right) along the loop. The heating rate for the loop shown is characterized by $F_{m0} = 151 \text{ W m}^{-2}$ and a scale height of $H_m = 1.25 \text{ Mm}$.

3.2. Loop evolution

Starting from the loop described above, we prescribe a *time-independent* heating function as given by Eq. (1) with a damping length of $H_m = 1.25 \text{ Mm}$, which results in a heating rate at the loop center that is 15% of the maximal heating rate, $Q_m(z_1)$. At $z = z_1 = 1.75 \text{ Mm}$, the ratio of mechanical heating to radiative losses is 0.26 at $t = 0$, while at the loop apex, it is 2.10. The evolution of the loop temperature, velocity, and density is shown in Fig. 1. During the first 2300 s the loop cools down from $T_{\text{top}}(t = 0) = 6.5 \cdot 10^5 \text{ K}$ to $T_{\text{top}}(t = 900 \text{ s}) = 2 \cdot 10^5 \text{ K}$, while the density stratification remains roughly constant. At $t = 2300 \text{ s}$ there is a sudden change: The temperature at the loop apex is no longer the maximal loop temperature, and this dip in the temperature stratification amplifies rapidly. At the same time, a flow towards the cooling loop apex sets in, which reaches $v \approx 2 \text{ km/s}$ at $t = 3200 \text{ s}$. At $t = 3400 \text{ s}$, a clump of cool (10^4 K) material with rapidly increasing mass content has formed at the loop apex. This clump, which we call the *condensation region* hereafter, eventually starts moving slowly towards one loop leg and is accelerated to $v \approx 3 \text{ km/s}$ before draining into the chromosphere at $t = 5300 \text{ s}$. As a result, a weak rebound shock forms on the left side, followed by a phase of chromospheric evaporation which refills the evacuated loop with plasma. This upflow decreases with time from $v(t = 5400 \text{ s}) \approx 1.5 \text{ km/s}$ to $v(t = 8000 \text{ s}) \approx 0$. In the mean time, the apex temperature of the loop has reached its maximum of $T_{\text{max,top}} = 3.4 \cdot 10^5 \text{ K}$ at $t = 7200 \text{ s}$. The subsequent decline in temperature is first slow and then becomes faster towards $t = 10\,000 \text{ s}$. At this time a dip in the temperature profile forms again at the loop apex, and the whole process

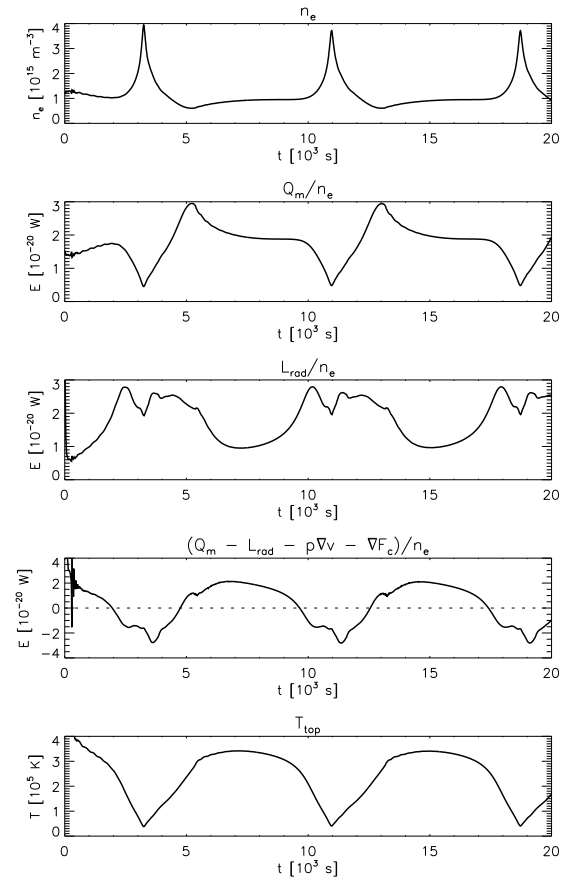


Figure 2. Energy balance at the loop apex for a damping length of $H_m = 1.25 \text{ Mm}$. From top to bottom: Electron density, n_e , mechanical heating per particle, radiative losses per particle, the sum $(Q_m - L_{\text{rad}} - p \nabla v - \nabla F_c)/n_e$ per particle (negative values mean that the loop apex is losing energy), and the temperature at the loop top.

repeats.

3.3. Energy balance analysis

The formation of the central dip of the temperature stratification results from the concentration of heating near the footpoints of the loop or, to put it differently, from insufficient heating at the top. In order to better understand the evolution of the loop, let us consider the energy balance at the loop apex for a damping length of $H_m = 1.25 \text{ Mm}$. The relevant terms for this are the mechanical energy supply, Q_m , the radiative losses, L_{rad} , the adiabatic compression, $p \nabla v$, and the divergence of the conductive flux, ∇F_c . As the density in the coronal part of the loop increases, the mechanical heating *per particle*, Q_m/n_e , decreases (the ion density, n_{ion} , equals approximately the electron density, n_e). This is displayed in the top row of Fig. 2. At the same time, the radiative losses per particle, L_{rad}/n_e (Fig. 2, center), increase as the temperature drops to $T = 2 \cdot 10^5 \text{ K}$, which is predominantly due to the temperature dependence of the radiative losses.

The time-dependence of the total energy balance at the

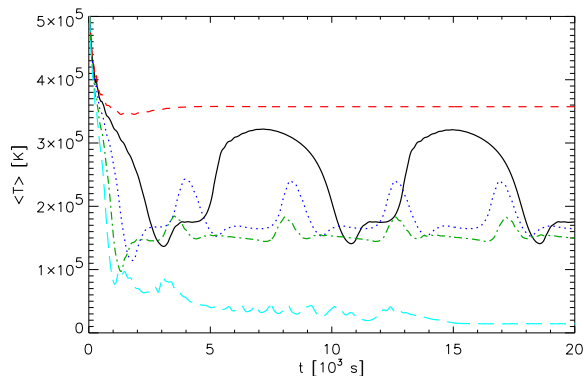


Figure 3. The influence of the damping length, H_m , on the thermal evolution of the loop. Dashed line: $H_m = 1.5$ Mm, solid line: $H_m = 1.25$ Mm, dotted line: $H_m = 1.0$ Mm, dash-dotted line: $H_m = 0.75$ Mm, long-dashed line: $H_m = 0.5$ Mm.

apex is dominated by two interacting processes, namely the increase of radiative losses and the increase of density. The *bottom* plot of Fig. 2 shows that, as a result of this interplay, the energy supply at the loop top becomes negative at $t = 2000$ s, which explains the developing dip in the temperature profile. The simultaneous decrease of the gas pressure initiates a symmetric flow towards the center of the loop, so that more and more mass is advected and a condensation region forms. Once the temperature dip has formed as a consequence of the described loss of equilibrium, a thermal instability sets in as $L_{\text{rad}} \propto n_e^2$. This process of runaway-cooling has been described, e.g., by Antiochos & Klimchuk (1991). As our model loop is of semicircular shape, the configuration with a condensation region located at the very center of the loop is gravitationally unstable. Therefore, the slightest perturbation forces the condensation region to move downward in either direction, where it experiences increasing acceleration as described below.

3.4. The role of the damping length

A plausible hypothesis is that the major factor in determining the cyclic behavior of the loop lies in the damping length, H_m , of the heating function because this critically influences the heat deposition at the loop top. We have studied the influence of the damping length on the thermal evolution of the loop by varying H_m from 0.25 Mm to 3.25 Mm and in each case letting the loop model evolve for 20 000 s. The temporal evolution of the mean loop temperatures, $\langle T \rangle$, for different values of the damping length, H_m , is displayed in Fig. 3. For this plot, we define the mean temperature as the average temperature over the central half of the loop, i.e. from $z = 2.5$ Mm to $z = 7.5$ Mm. Let us consider the limiting cases first: For short damping lengths of $H_m \lesssim 0.5$ Mm, the loop decays as not enough energy is deposited in the upper part of the loop to balance the radiative and conductive losses. In this case the temperature in the loop falls during the first 15 000 s to roughly 10^4 K and stays at that level for the remainder of the model run, maintained in part by the

“opacity” heating term. On the other hand, for longer damping lengths with $H_m \geq 1.5$ Mm, the energy deposition at the loop center is large enough to sustain a stable loop against radiative and conductive losses and an average loop temperature of $3.6 \cdot 10^5$ K (for $H_m = 1.5$ Mm) is reached and maintained (see Fig. 3, *dashed*). Even longer damping lengths lead to stable loops with slightly higher temperatures. The regime in between, with intermediate damping lengths of $0.75 \text{ Mm} \leq H_m < 1.5 \text{ Mm}$, shows the cyclic behavior described above. In these cases, the loop exhibits a dynamic behavior, triggered by the onset of thermal instability as described in Sect. 3.2.

As shown in Fig. 3, the period of the condensation cycle depends on the damping length – the more the heating is localized near the footpoints, the sooner the thermal instability sets in.

3.5. Limit cycle of loop evolution

As pointed out previously, the thermal evolution of the model coronal loop shows periodicity for a significant parameter range of the damping length. To illustrate this cyclic pattern, we plot in Fig. 4 the mean density, $\langle \rho \rangle$, of the loop as a function of mean loop temperature, $\langle T \rangle$.¹ Fig. 4 displays the loop evolution for two different damping lengths: For $H_m = 1.50$ Mm, the loop approaches a stationary solution (*open circles*), while for $H_m = 1.25$ Mm (*dots*), the loop enters a limit cycle after its initial cooling, expressing the fact that the loop evolution becomes independent of the initial boundary conditions. The evolution can be divided into four parts:

- I The 10 Mm loop first cools down from its initial mean temperature of $\langle T \rangle_0 = 5 \cdot 10^5$ K to $\langle T \rangle \approx 1.4 \cdot 10^5$ K.
- II a The onset of condensation is seen as an increase in the mean density of the loop. The mean temperature starts to rise again shortly before the condensation region leaves the loop, which is due to the fact that one side of the loop is already reheating while the condensation region is moving to the other side. The stage of evolution when the condensation region drains from the loop is seen as a sudden drop in density from $\langle \rho \rangle = 3.6 \cdot 10^{-12} \text{ kg m}^{-3}$ to $\langle \rho \rangle = 1.4 \cdot 10^{-12} \text{ kg m}^{-3}$. One point is plotted for each 10 s of the evolution, and the lack of points in this fairly large interval of mean density illustrates that the condensation region leaves the loop very quickly (but still with a velocity that is much slower the free-fall velocity of $v_{\text{ff}} = 31.2 \text{ km/s}$ for this loop).

¹From here on, we define the mean values as the average quantities over the region of the loop which lies above the transition region, bounded by the points where the temperature crosses $T = 10^5$ K in both loop legs. The exact choice of this cut-off value does not significantly influence the results. In contrast to the convention used in the previous section, this definition is independent of motions of the chromosphere–transition region boundary, while the former definition was used to describe the loop cooling down to $T \approx 10^4$ K together with the oscillating and “hot” loop solutions.

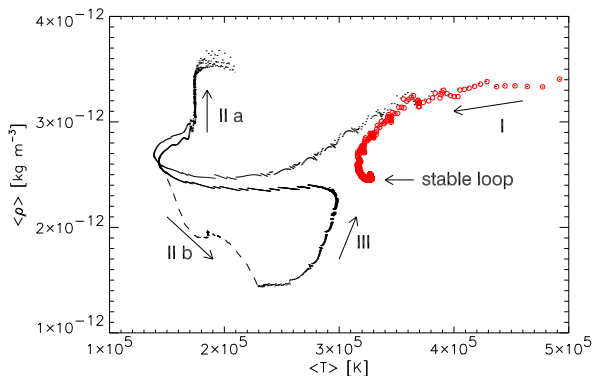


Figure 4. Limit cycle of loop evolution for a damping length of $H_m = 1.25 \text{ Mm}$ (dots) and $H_m = 1.50 \text{ Mm}$ (open circles). The phases of evolution are indicated as follows: (I): initial cooling, (II a) condensation, (II b) simultaneous evolution of the hot part of the loop (dashed line), (III) loop reheating and chromospheric evaporation.

II b As the mean density of the loop during the condensation phase is dominated by the condensation region itself, we also evaluated the density in the hot part of the loop alone: Due to the formation of a condensation region, the density in the adjacent parts of the coronal loop decreases which leads to an increase in temperature. The mean values of the hot part of the loop for this stage of evolution is plotted as a *dashed line* in Fig. 4.

III After the condensation region has drained, the evacuated loop reheats and chromospheric matter is evaporated, as indicated by the increase in mean density. When the loop reaches $\langle T \rangle = 3 \cdot 10^5 \text{ K}$, the radiative losses at the loop top are no longer balanced by the energy supply through mechanical heating, conductive flux, and enthalpy flux, so that the temperature starts to decrease and the cycle repeats.

Cyclic evolution of coronal loops was studied for the first time by Kuin & Martens (1982). In their semi-analytical model, they treated the coronal loop as a zero dimensional system, coupled to the underlying chromosphere. Depending on the strength of the coupling, the authors obtained different classes of solutions, namely solutions converging towards a fixed point, and solutions approaching a limit cycle. As the loop was treated as one zero dimensional system, however, Kuin & Martens were not able to model any spatially localized condensation which in our work leads to the upward-arching branch in the $\langle \rho \rangle(\langle T \rangle)$ diagram of Fig. 4. Considering the hot coronal part of the loop alone, in contrast, reconciles our spatially resolved loop model with the semi-analytical approach of Kuin & Martens (cf. Fig. 4, *dashed line*).

3.6. Spectral signature of condensation in transition region lines

The fact that our numerical code self-consistently solves the non-equilibrium ionization rate equations not only for hydrogen and helium, but also for the atomic species C, O (and Fe, Mg, N, Ne, and Si, if desired) offers the possibility of synthesizing optically thin transition region lines. The inclusion of non-equilibrium ionization effects is of vital importance when studying the spectral signature of a plasma in a *dynamic* state like in the present case.

Fig. 5 displays the intensity variations of the lines C IV (154.8 nm) (formation temperature $T_f \approx 1 \cdot 10^5 \text{ K}$), O V (63.0 nm) ($T_f \approx 2.2 \cdot 10^5 \text{ K}$), and O VI (103.2 nm) ($T_f \approx 3.2 \cdot 10^5 \text{ K}$) during the evolution of the loop. The spectral lines are calculated by integrating the emission of the entire loop as seen vertically from the top, the line widths are given in velocity units. All three lines show periodic brightenings which have their origin in the condensation process. In the case of the C IV line, the strong increase in density at the beginning of the condensation results in high radiative losses and hence an intensity maximum. A second maximum of slightly smaller amplitude is attained when the condensation region has grown to its maximum, shortly before draining down the loop leg. Right after the condensation region has left the loop, the intensity is minimal as the loop is devoid of plasma at this stage. In the following evolution, the intensity gradually increases as chromospheric evaporation sets in again. In contrast to this, the intensity of the O VI line is maximal when the temperature is highest as the line is formed around $T_f \approx 3.2 \cdot 10^5 \text{ K}$. When the condensation sets in and the maximal loop temperature temporarily sinks below $T = 2 \cdot 10^5 \text{ K}$, the intensity in O VI almost drops to zero. The O V line, formed around $T_f \approx 2.2 \cdot 10^5 \text{ K}$, can be considered as an intermediate case.

4. DISCUSSION

We have shown that cool coronal loops can exhibit inherently dynamic behavior even under the simple assumption of a mechanical energy flux into the loop that is dissipated exponentially with a given scale height but constant in time. This scenario is interesting in the sense that no time-dependent driving mechanism is needed to generate transient brightenings in transition region lines. Simultaneous observations of, e.g., the C IV (154.8 nm) and the O VI (103.2 nm) lines, would be advantageous in order to verify if this phenomenon is as ubiquitous as it seems.

Recent TRACE observations of Schrijver (2001) indeed show frequent “catastrophic cooling” and evacuation of coronal loops over active regions and enhanced emission of C IV, developing initially near the loop top, followed by quick draining. Furthermore, CDS observations by Fredvik (2002, private communication) show localized brightenings in coronal loops in O V (63.0 nm) above the limb which move quickly towards the solar surface and could be interpreted as cooling plasma close to a condensation region. In the second part of this work (Müller

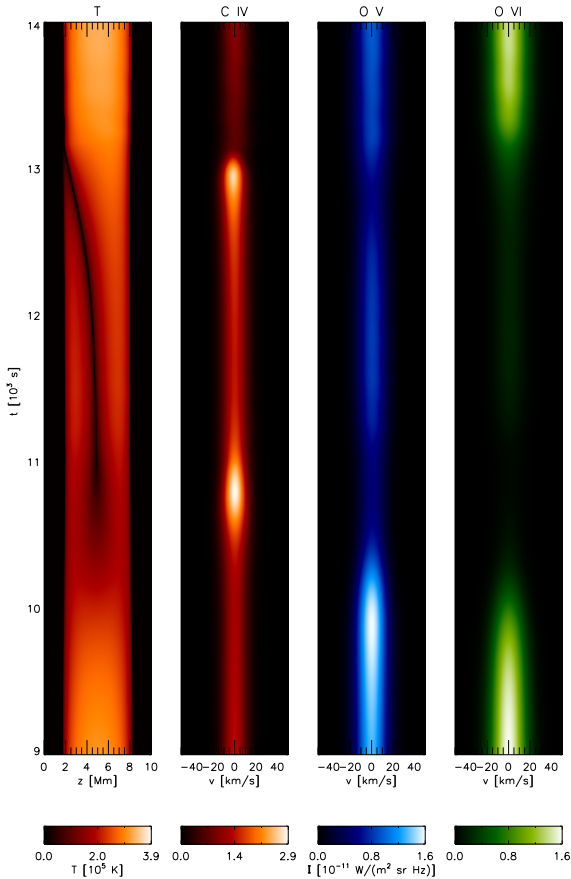


Figure 5. From left to right: Space-time plot of the loop temperature and the corresponding variations of the lines of C IV (154.8 nm), O V (63.0 nm), O VI (103.2 nm) for a damping length of $H_m = 1.25$ Mm.

et al., 2003b), we present the first results of catastrophic cooling in long coronal loops.

The fact that the dynamic loop models described in this work can show strong emission in lines formed at $T \leq 10^5$ K and at the same time relatively weak emission in lines formed at higher temperatures seems promising with respect to the outstanding problem that current models predict an emission measure that is either much lower than the emission observed at $T < 10^5$ K or much higher than what is observed at $T > 10^5$ K. Further observational confirmation of the dynamics predicted in this paper, preferably concentrating on shorter loops, would lead to a strengthening of the hypothesis that coronal heating is concentrated towards the footpoints of loops. Such knowledge would be very useful to limit the number of possible coronal heating mechanisms.

REFERENCES

- Antiochos, S. K. & Klimchuk, J. A. 1991, *ApJ*, 378, 372
 Antiochos, S. K., MacNeice, P. J., & Spicer, D. S. 2000, *ApJ*, 536, 494
 Antiochos, S. K., MacNeice, P. J., Spicer, D. S., & Klimchuk, J. A. 1999, *ApJ*, 512, 985

- Antiochos, S. K. & Noci, G. 1986, *ApJ*, 301, 440
 Aschwanden, M. J., Nightingale, R. W., & Alexander, D. 2000, *ApJ*, 541, 1059
 Aschwanden, M. J., Schrijver, C. J., & Alexander, D. 2001, *ApJ*, 550, 1036
 Cally, P. S. 1990, *ApJ*, 355, 693
 Cally, P. S. & Robb, T. D. 1991, *ApJ*, 372, 329
 Dowdy, J. F., Rabin, D., & Moore, R. L. 1986, *Sol. Phys.*, 105, 35
 Gudiksen, B. V. & Nordlund, Å. 2002, *ApJ*, 572, L113
 Hansteen, V. 1993, *ApJ*, 402, 741
 Hansteen, V. H. & Leer, E. 1995, *J. Geophys. Res.*, 100, 21577
 Karpen, J. T., Antiochos, S. K., Hohensee, M., Klimchuk, J. A., & MacNeice, P. J. 2001, *ApJ*, 553, L85
 Kuin, N. P. M. & Martens, P. C. H. 1982, *A&A*, 108, L1
 Mariska, J. T. 1992, *The solar transition region* (Cambridge Astrophysics Series, New York: Cambridge University Press, 1992)
 Müller, D. A. N., Hansteen, V., & Peter, H. 2003a, *A&A*, in press
 Müller, D. A. N., Peter, H., & Hansteen, V. 2003b, in *Proceedings of the SOHO-15 workshop*, ed. H. Lacoste (ESA SP-547), these proceedings
 Peter, H. & Judge, P. G. 1999, *ApJ*, 522, 1148
 Rosner, R., Tucker, W. H., & Vaiana, G. S. 1978, *ApJ*, 220, 643
 Schrijver, C. J. 2001, *Sol. Phys.*, 198, 325
 Serio, S., Peres, G., Vaiana, G. S., Golub, L., & Rosner, R. 1981, *ApJ*, 243, 288
 Spitzer, L. 1962, *Physics of Fully Ionized Gases* (New York: Interscience (2nd edition))
 Vernazza, J. E., Avrett, E. H., & Loeser, R. 1981, *ApJS*, 45, 635